The application of low energy electron microscopy and photoemission electron microscopy to organic thin films

2008 J. Phys.: Condens. Matter 20 184007

(http://iopscience.iop.org/0953-8984/20/18/184007)

J. Phys.: Condens. Matter **20** (2008) 184007 (12pp) doi:10.1088/0953-8984/20/18/184007

The application of low energy electron microscopy and photoemission electron microscopy to organic thin films

Frank-J Meyer zu Heringdorf

Department of Physics and Center for Nanointegration Duisburg-Essen (CeNIDE), Lotharstrasse 1, 47048 Duisburg, Germany

E-mail: meyerzh@uni-due.de

Received 21 February 2008, in final form 16 March 2008
Published 17 April 2008
Online at stacks.iop.org/JPhysCM/20/184007

Abstract

Over the last few years, low energy electron microscopy and photoemission electron microscopy have been successfully used to study the growth dynamics of various organic semiconductors. In the present work, the recent advances in the application of surface sensitive electron microscopy techniques to organic thin films are reviewed, and the requirements for successful imaging of organic molecules in low energy electron microscopy and photoemission electron microscopy are discussed. Starting from a discussion of the basic design features of the microscopes, a variety of imaging modes are presented to illustrate the type of information that can be gained from *in situ* surface sensitive electron microscopy. In photoemission microscopy, the contrast greatly depends on the illumination source that is used for imaging. Using a frequency doubled femtosecond Ti:sapphire laser as a light source for photoemission, even electronic states within the molecules can be directly used for imaging in two-photon photoemission electron microscopy. The article focuses on the two linearly conjugated molecules pentacene ($C_{22}H_{14}$) and anthracene ($C_{14}H_{10}$) as model systems.

(Some figures in this article are in colour only in the electronic version)

1. Introduction

Organic semiconductors have in the last few years shown their enormous potential, with first applications on the market and with many visions for future applications being developed every day. The high potential of organic materials is that in most cases the processing can be performed at a temperature close to room temperature, which provides for plastic substrates that are lightweight and flexible. Devices in organic semiconductors have been developed that reach charge carrier mobilities comparable to mobilities found in amorphous silicon and inspire fantasies of radio frequency identification tags (RFIDs) or even simple computing in organics. Displays based on organic semiconductors are lighter than today's thin film transistor (TFT) display panels that are used for television sets and liquid crystal display (LCD) monitors. As they produce light with organic light emitting diodes (OLEDs), organic displays will not rely on backlighting, either. Such displays consume less power, have a greater contrast, and can be read even in bright sunlight. They have been used in car radios and displays for cell phones for years, but only recently were the first larger organic display panels announced. Naturally, with the diversity of applications—computing, RFIDs and displays—different organic semiconductors, organic interfactants and surfactants, and materials for contacts have to be combined. Accordingly the growth properties of organic materials on plastic, glass, or even silicon become an important issue. The surface science of organic semiconductors, however, is still just at the beginning. This has a variety of reasons. Polymers, for instance, that are frequently used in organic displays, usually do not form crystals and as a result are hard to analyze with the standard toolkit of surface science that typically focuses on crystalline materials. Other organic materials do form crystalline structures, but are very fragile. For instance, the molecule pentacene, as will be shown later, if deposited on Si, forms beautiful crystals with a size of several tens of microns. If one attempts to obtain a low energy electron

diffraction (LEED) pattern, however, the film immediately gets severely damaged. Other troubles are caused by charging of the typically used glass or indium tin oxide (ITO) substrates. Accordingly, numerous studies of organic materials have been performed with scanning tunneling microscopy (STM), with atomic force microscopy (AFM), with x-ray diffraction, and with ultraviolet photoemission spectroscopy. Another very popular approach is to grow field effect transistors and then simply judge the film quality by measuring the device performance, i.e., by determining the electron (or hole) mobility in the device. None of the techniques discussed is fast enough to be easily adapted to an experiment during deposition, though. This article focuses on a technique that has been successfully used for *in situ* studies, i.e., investigations during growth, of several organic materials. Low energy electron microscopy (LEEM) provides for surface sensitive imaging with low electron doses and—even more important—utilizes electrons of an energy that is almost zero. A similar technique, photoemission electron microscopy (PEEM), makes use of the photoelectric effect and can thus be combined with a variety of different light sources to obtain contrast. For imaging of organic semiconductors, a simple laboratory Hg discharge lamp with an energy cutoff of ≈4.9 eV or a high flux He lamp is already sufficient. Femtosecond laser sources can also be used for illumination, although the photon energy is usually not sufficient for photoemission, and two-photon processes are required. As photoemission must proceed through an intermediate state in this case, careful selection of the laser wavelength (and the materials system) allows one to perform *in situ* microscopy of excitons inside the organic material during growth.

In the remainder, a brief introduction to the methodology will be given, followed by two examples in which the technique has been successfully exploited for imaging of the organic material during growth.

1.1. Experimental considerations

One of the big advantages of LEEM and PEEM is that—in contrast to other popular electron microscopy techniques like scanning electron microscopy or transmission electron microscopy—the microscopes are typically ultrahigh vacuum (UHV) tools with transfer systems, heating (and sometimes cooling stages) as well as preparation chambers that provide excellent control over the surface cleanliness and morphology. Inside the microscopes, the line of sight to the sample surface allows the *in situ* deposition of thin films. The resulting data set in this case is a movie of the growth process that can be analyzed frame by frame. The microscopes, available from various vendors, differ in achievable resolution, energy filtering capabilities, sample holder design, cooling options, and many electron-optical subtleties. A detailed discussion of the broad spectrum of available instruments would clearly go beyond the scope of this article. Most of the microscopes, however, share some contrast mechanisms that are important for the imaging of organic thin films. In the following, a brief description of a typical setup will be given.

First, it is important to distinguish between LEEM and PEEM. A typical setup for the electron optics of a LEEM,

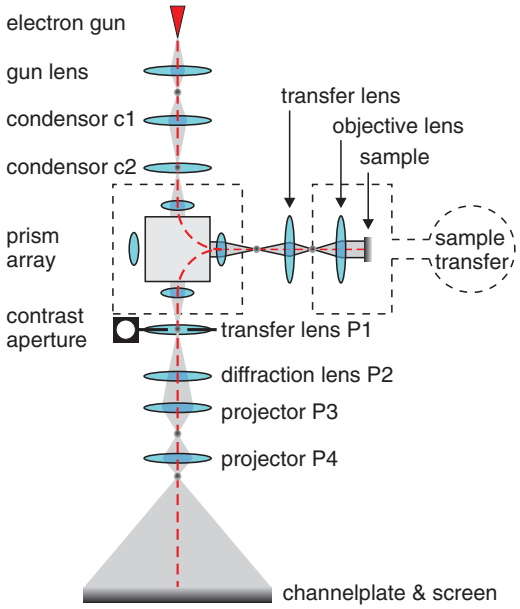

Figure 1. Experimental setup of the IBM LEEM II, after [1]. A field emission electron gun at the top of the microscope creates an electron beam that travels down the illumination column, becomes deflected by the prism array, and is diffracted at the surface. The reflected beam re-enters the prism array and is deflected downwards into the imaging column, where the final magnification is achieved. The surface sensitivity is obtained by decelerating of the electrons between the objective lens and the sample to an energy of almost 0 eV. If the electron gun is switched off and the surface is illuminated with light, photoelectrons can be imaged (PEEM). Other electron-optical designs are also possible [2–4], some of which have been successfully applied in the growth of organic semiconductors.

the IBM LEEM II [1], is shown in figure 1. At the top of the microscope, a standard UHV scanning electron microscope (SEM) electron gun is used to create a highly coherent electron beam that travels down the column with an energy of 15–20 keV. The electron beam is bent to the right by a magnetic prism and is focused into the back focal plane of the objective lens. The objective lens creates a parallel beam of electrons that—after proper alignment of the microscope—impinges perpendicularly onto the sample surface. As low energy electrons are desired, the sample is held at a high voltage potential similar to the acceleration voltage of the electron gun. Accordingly, the electrons arrive at the sample surface with a difference energy close to 0 eV and are reflected or—at a slightly higher relative electron energy—diffracted by the sample surface. After the interaction with the surface, the electrons are again accelerated towards the objective lens and both the image plane and the diffraction pattern are transferred through the beam splitter and downwards into the imaging column. In particular, the diffraction pattern is located in the center of the transfer lens P1, where an aperture can be inserted to select diffraction spots for dark-field imaging. The diffraction lens P2 allows switching between the diffraction pattern and the real space image. The final magnification of the image/diffraction pattern is achieved by a set of projection lenses (P3, P4). Ultimately, depending on the setting of the diffraction lens P2, either the image plane or

the diffraction pattern becomes intensified by a multi-channel plate and recorded with a slow scan scientific CCD camera. Different operation modes of the instrument are possible that are described in various places throughout the literature [5–7]. For basic imaging, the capabilities include the so-called mirror mode imaging, where the electron energy is lowered so much that the electrons are reflected at the outer potential of the surface before diffraction takes place. In bright-field imaging, only the central LEED spot is used for imaging, while under dark-field conditions any other LEED spot is used. Multi-beam imaging conditions, as used in transmission electron microscopy, only recently became feasible by implementation of aberration correctors, which are so far only installed in very few instruments. The lateral resolution of state-of-the-art commercial LEEMs is slightly better than 5 nm laterally [1], with special aberration corrected designs aiming at 2 nm [8]. The vertical resolution, however, is much higher due to diffraction contrast, and under dark-field conditions or phase contrast, atomic steps on a Si surface can be easily resolved. Furthermore, the *in situ* capabilities of LEEM allow heating and (in some designs) cooling of the samples during deposition and image acquisition with video rate.

If the electron gun of a LEEM is switched off and the sample surface is illuminated with light instead, photoemission can take place if the photon energy of the light is sufficiently high to overcome the photoelectric work function of the structures on the sample. As the electron optics of the microscope is designed for the imaging of low energy electrons, the photoemitted electrons are accelerated from the sample towards the objective lens by the bias voltage of the microscope, form a representation of the photoemitted electron angular distribution (PEEAD) in the back focal plane of the objective lens, and ultimately form a PEEM image on the screen. While in LEEM the possible field of view is commonly limited by the achievable size of the electron spot on the sample, in PEEM such a restriction does not exist and imaging can take place with fields of view of 100 μm, as will be demonstrated later. The contrast mechanism in PEEM is completely different from the contrast in LEEM, and PEEM is per se not necessarily sensitive to topographical information. If local electronic differences exist on the surface, however, PEEM is excellently suited to exploit such differences to resolve even single-molecule-high layers. By combining microscopes with imaging energy filters [2] the local electronic differences can be quantified on the nanoscale with an energy resolution of typically less than 0.3 eV.

Microscopes installed in user facilities typically provide all the possibilities described so far and very often form end stations of a synchrotron beamline. For laboratory experiments, however, pure PEEMs are very popular. These are simpler microscopes without a prism array and an electron gun, i.e., they can be built as flange-on microscopes (although they are usually mounted on dedicated chambers). Such microscopes are on the one hand significantly cheaper than LEEMs, but on the other hand offer a smaller number of contrast mechanisms.

For imaging of organic molecules, beam damage is an important issue. Organic materials can easily be damaged by too high an electron dose and are usually temperature sensitive as well. Figure 2 illustrates what happens if a several molecules thick pentacene film is irradiated with UV light from a Hg discharge lamp. After only a few seconds holes start to show up in the film that gradually grow larger and deeper until the film is severely damaged, and is almost completely evaporated in the end. Interestingly, under synchrotron radiation, pentacene films appear stable for hours, and the film can also be imaged for extended periods of time under illumination with a laser, without the presence of features as displayed in figure 2. It is believed that the infrared parts of the spectrum of the Hg discharge lamp are responsible for the beam damage [9], and the easiest way to circumvent the beam damage is to limit the total exposure of the film to the light. During slow deposition, it is sufficient to record images only once a minute and in between the exposures the light can be switched off by an electronic shutter. The control of such a shutter can be synchronized to the acquisition software of the microscope. This technique has been applied for all growth studies presented here that use a Hg discharge lamp for illumination. By minimizing the exposure of the film to the UV light, the beam damage can be minimized and imaging is possible for hours without changes in the film's morphology.

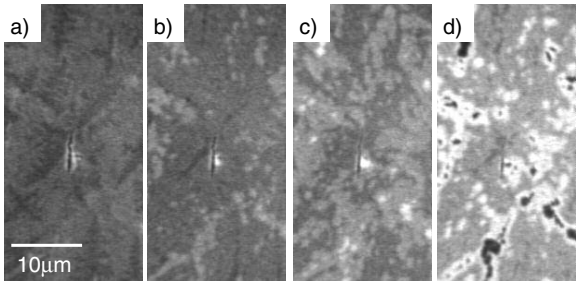

Figure 2. Sequence of images illustrating the damage of a pentacene film by light from a Hg discharge lamp. After [9].

In the following sections, LEEM and PEEM studies of pentacene and anthracene will be reviewed to demonstrate what types of information can be gained from the application of surface sensitive electron microscopy when organic molecules are of interest. An additional section will focus on a novel type of experiment, where femtosecond laser pulses are used to visualize excited electronic states within the molecules by means of two-photon photoemission.

2. Pentacene

Pentacene ($C_{22}H_{14}$) is a polycyclic hydrocarbon that is composed of five linearly fused aromatic rings. Pentacene has attracted great attention over the last few years due to its enormous potential for organic circuit use and has been extensively studied. Pentacene also was amongst the first molecules that were successfully studied with PEEM [10].

2.1. Growth on Si surfaces

Figure 3 shows images of a growing pentacene film on Si(001) during deposition at room temperature. The three bright and

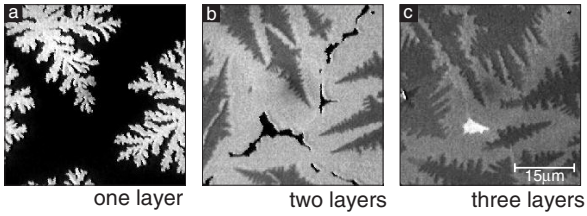

Figure 3. Sequence of images recorded during growth of pentacene on Si(001). (a) Formation of the first islands, (b) second-layer formation, (c) topography of a three-layer-high film. After [9].

fractal-shaped islands in panel (a) are only one molecular layer high, as judged from the growth kinetics in PEEM. The molecules in the islands are standing up, with their long axis almost perpendicular to the surface plane, as can easily be confirmed, in *ex situ* AFM, by identification of a polymorph with a step height of 15.4 Å [11]. Apparently, the molecules form the so-called 'thin film phase' [12] of pentacene. In panel (b) of figure 3 a second layer of pentacene is formed on top of the first layer. This layer appears darker and shows a higher nucleation density, as on each of the first-layer islands several second-layer islands are nucleated. Interestingly, all second-layer islands that are nucleated on top of the same island in the first layer show a similar preferential direction of growth, indicating that there exists some epitaxial relation between the first and the second layer. In panel (c) of figure 3 the three-layer-high islands appear darker than both the second layer and the first layer. During continued growth, the brightness of the layers exponentially decreases as a function of the layer's thickness, and after approximately six layers the contrast between subsequent layers has become so weak that the layers cannot be reliably distinguished any longer. The PEEM image then appears homogeneously gray. A detailed analysis of the contrast mechanism would require either energy filtered PEEM or integral photoemission measurements. Such measurements of pentacene deposited on the Si(111) surface found that an interface dipole is formed during the adsorption of the first layer, which lowers the ionization potential of the surface by 0.55 eV [13]. At the same time, the C 1s core level shifts to higher binding energies, which was interpreted as a charge transfer from the molecule to the substrate. At higher coverages, however, the C 1s core level shifts back to lower binding energies and ultimately reaches its old value. While it is impossible to quantitatively compare the different studies due to incompatible monolayer definitions, the completed recovery of the C 1s level is most likely the situation when the layers cannot be distinguished in PEEM any more. Hence, while it is hardly possible to determine the surface morphology of a thicker pentacene film, PEEM is excellently suited to analyzing the growth dynamics of the first few layers.

Figure 4 shows the filling of the first three layers of pentacene as a function of the integral amount of deposited material [10]. Not surprisingly, the film starts to build up a slight roughness during growth, as the second and third layers are started before the first and second layer are completely closed. More interestingly, the first layer is only formed after an initial 'dead-time' during which approximately 0.2 ML of

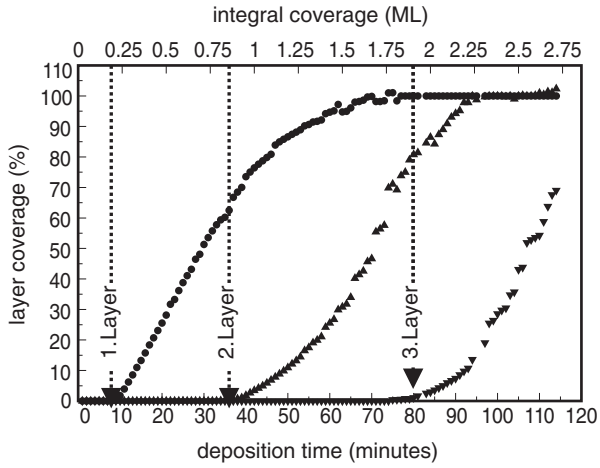

Figure 4. Relative coverage of pentacene in the first layers as a function of the deposition time. After the beginning of the deposition, 0.2 ML of pentacene are adsorbed on the surface before the first islands become visible. After [10].

material have been deposited (a closed monolayer is defined here as the amount of material that is needed to completely fill the surface with bright first-layer islands, counted from the first occurrence of first-layer islands). One would speculate immediately that the material could be in a lattice gas on the surface and after reaching a certain saturation coverage assembles into islands. The linear dependence of the filling in the first layer after the first bright islands are formed, however, indicates that the 0.2 ML remain on the surface and become buried under the film. On the basis of low coverage STM investigations [14, 15] it was proposed [10] that the missing 0.2 ML remain below the islands and consist of flat lying molecules that covalently bind to the substrate and passivate the Si dangling bonds. After the covalent binding of the pentacene molecules to the Si was suppressed by deposition of another organic molecule (cyclohexene) prior to the pentacene growth, the initial dead-time vanished. It was later concluded from infrared absorption spectroscopy that during the initial adsorption of pentacene on Si(001) some of the carbon atoms in the molecule undergo a change from sp_2 to sp_3 hybridization and indeed form a strong covalent bond to the dangling bonds of the Si substrate [16]. A similar mechanism was also found for other crystallographic surfaces of Si [17]. The flat lying layer of chemisorbed molecules that shields the growing film from the substrate thus seems to be a general concept for the system pentacene/Si, and it is not surprising that as a result of this self-interfactant effect [18], the morphology of the films is independent of the orientation of the Si substrate.

The covalent nature of the bond to the Si surface will also play an important role if the growth of pentacene on Si is compared to the growth of pentacene on metallic surfaces.

2.2. *Electron diffraction*

The crystalline quality of the films can also be analyzed using low energy electron diffraction (LEED). The aforementioned beam damage of the films is an important issue during such investigations. Using a regular rear-view LEED optics can

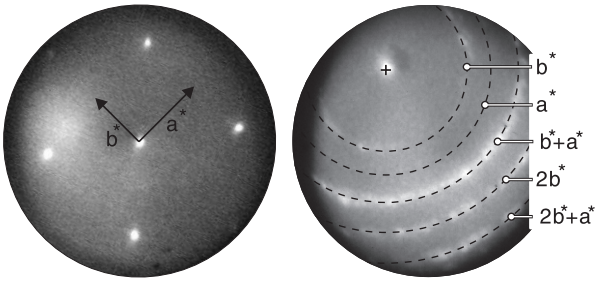

Figure 5. LEED patterns of thin pentacene films recorded with LEEM. (a) Diffraction pattern of a single pentacene island, showing the characteristic pentacene LEED pattern, (b) tilted LEED pattern of a larger area on the surface. The diffraction rings are concentric around the specular spot and reflect the textured composition of the film. All ring positions can be explained with linear combinations of the reciprocal lattice vectors $a^\star$ and $b^\star$.

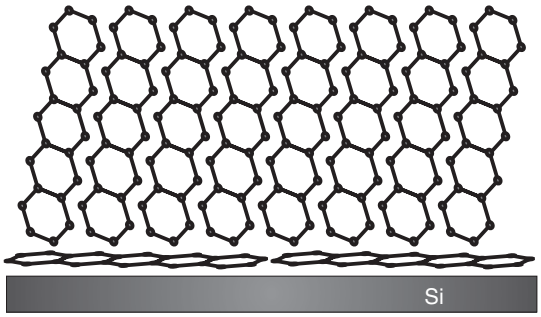

Figure 6. Growth of pentacene on Si. Initially a flat lying layer of molecules is formed that subsequently becomes buried under a film of molecules standing up.

easily result in beam damage. Multi-channel plate LEED instruments that use extremely low electron doses, and which are especially designed for electron diffraction of organic molecules, do not, in the case of pentacene, offer a satisfying solution. With lattice vectors of $a = 5.9$ Å and $b = 7.6$ Å [19], diffraction spots are expected under angles that can—in a regular rear-view LEED geometry—only be imaged on the screen at electron energies well above the damaging threshold. During the deposition of pentacene on a Si(111) surface, for instance, the LEED spots of the substrate will simply disappear during adsorption of the flat lying layer of molecules, but a pentacene-related pattern will not appear, even for thicker pentacene layers.

The electron optics of the LEEM, on the other hand, allows the recording of diffraction patterns at low energies and with low beam damage. In contrast to a regular LEED optics case, the spot positions of the diffraction spots in the LEED mode of the LEEM are independent of the electron energy. The visible part of the LEED pattern at low energies is thus not limited by the amount of the diffraction pattern that can be viewed on the screen, but by the size of the Ewald sphere. Figure 5 shows LEED patterns of pentacene films on Si(100) and Si(111) that were recorded with a LEEM instrument operated in LEED mode. In panel (a) the electron beam was confined to the size of a single pentacene island, and the resulting diffraction pattern corresponds to the diffraction pattern of a single island. The arrows in panel (a) of figure 5 indicate the unit vectors [20] of the pentacene thin film phase. Moving the electron beam from island to island reflects the textured nature of the film: the diffraction patterns of all islands are similar, but they are rotated with respect to each other by arbitrary angles. This is illustrated in figure 5(b), where a larger electron beam was tilted in the Ewald sphere to show higher diffraction orders without having to increase the electron energy. The rings around the central LEED spot (marked by a cross) can be fully explained by the thin film phase lattice vectors $a^\star$ and $b^\star$ and by linear combinations thereof. The pattern remains stable for minutes under the electron beam, as long as the electron energy is not raised above ∼15 eV, which causes the diffraction pattern to irreversibly fade within a second.

Figure 6 summarizes the interface formation between pentacene and the Si substrate: during adsorption of the first molecules a flat lying wetting layer is formed that remains at the interface and gets overgrown by higher layers. The higher layers consist of molecules that are standing up.

2.3. Island shapes and sizes

The *in situ* capabilities of PEEM give access to the island density and the shape development of the islands during growth. While the first layer of flat lying molecules most likely exhibits a hit-and-stick behavior, based on the strongly covalent nature of the bond between the molecule and the Si substrate, the layers standing up that appear bright in PEEM are several tens of micrometers in size, indicating that the diffusion length for molecules on the flat lying layer is quite large. The size and the nucleation density of the islands can be influenced by changing the substrate temperature and deposition rate. If, for instance, the deposition rate is increased during growth, additional islands nucleate on the surface between the islands already present because a higher deposition rate yields a larger nucleation density [9]. From the dependence of the nucleation density N_1 on the flux F [21],

$$N_1 = F^{i/(i+2)} \times \exp\left\{\frac{E^\star}{k_B T}\right\} \qquad (1)$$

with $E^\star$ as a weighted sum of the activation energies [9], it is possible to determine the critical nucleus size i. A stable island is formed when more than i molecules meet on the surface; an island consisting of i molecules or less may also decay again into independently diffusing entities. From PEEM experiments, $i \approx 6$ was claimed for pentacene on a cyclohexene saturated Si(001) surface [9]. Although this number has a huge error bar attached to it, it is in surprisingly good agreement with independent estimates of critical cluster sizes for pentacene on SiO_2 [22–24], pentacene on Al_2O_3, and pentacene on poly(methylmethacrylate) (PMMA) [25], which all yield critical island sizes between $i = 2$ and 4. In contrast to many classical systems, where just two atoms form a stable entity, in the case of pentacene several molecules are needed for an island to become stable. Again, this argument

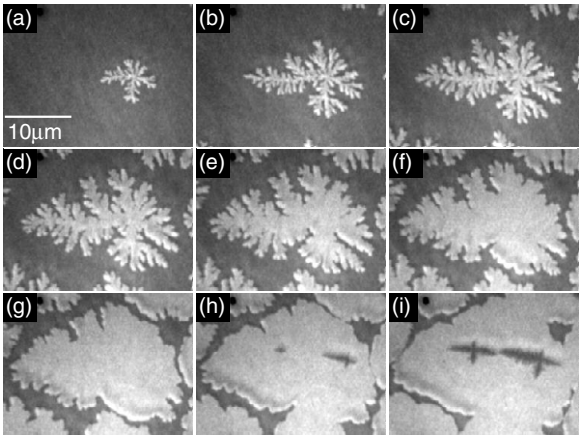

Figure 7. Sequence of PEEM images recorded during growth of pentacene on a Si(113) surface. (a) Formation of the first island; ((b), (c)) growth of the pentacene island with constant fractal dimension; ((d)–(i)) gradual increase of the fractal dimension of the pentacene island.

holds only for layers with molecules standing up, in which the molecule mobility is assumed to be significantly larger than in the first flat lying layer on Si, where the absence of morphological contrast in PEEM suggests a disordered layer and short diffusion lengths.

If the shape of the islands is considered, the first-layer islands of molecules standing up clearly consist of fractals. The fractal dimension of isolated pentacene islands, $D \approx 1.6$–1.7 [10], independent of the orientation of the Si substrate [18], suggests a growth mode that is determined by diffusion limited aggregation (DLA) [26]. However, the original DLA model does not take into account the specific situation of MBE growth, which was only added later to describe pentacene DLA on a surface. One of the important ramifications of this scenario, with a pentacene flux that is homogeneous throughout the field of observation, is that the fractal dimension does not remain constant for all coverages. This can easily be understood if one considers that the dimension of a closed layer is always $D = 2$, and that the initially isolated fractal pentacene islands will gradually approach each other with increasing coverage and will ultimately form a closed layer. Figure 7 shows the evolution of the shape of pentacene islands during growth for pentacene deposited on a Si(113) surface. In panels (a)–(c), the island in the center evolves almost freely, as it is far enough separated from surrounding islands. In panels (d)–(f), the island starts to compete with the surrounding islands for the molecules that are deposited between the islands. At the same time, while the island becomes bigger, a larger amount of material is deposited on top of the island. Since a second layer is not yet formed, the molecules that land on top of the island diffuse to the edge of the island and fill in the grooves in the fractal structure from within. This results in a rounding of the edges and consequently in an increase of the fractal dimension of the island. As the island grows, this mechanism becomes dominating, because the grooves between the islands become smaller and most of the new material is deposited on top of the island. Ultimately (panels (g)–(i)) this leads to a compact island and a fractal dimension close to $D = 2$, which is only reached once the layer is completely closed.

The dependence of the fractal dimension on the separation of the islands also explains why the shape of the islands depends on the substrate and on the flux, i.e., to be more precise, on the nucleation density. If, for instance, the deposition rate is increased, the diffusion length of the molecules on the surface will be unaffected, but the nucleation density will be higher (as a result of equation (1)) and more compact islands will be observed as the diffusion fields of the islands start to overlap at an earlier stage of growth. The same effect can be caused by heterogeneous nucleation at defect sites. Accordingly, while nicely separated fractals are usually observed on Si substrates, smaller and more compact islands are observed on SiO_2.

2.4. Metallic substrates

While deposition of pentacene on Si surfaces usually yields the thin film phase, the outcome can be very different if pentacene is deposited on metals. With scanning tunneling microscopy it was observed for several metals (e.g., Au(111) [27], Cu(111) [28] and Ag(110) [29]) that the pentacene molecules predominantly lie flat on the surface, independently of the thickness of the film. This is quite different from the case for pentacene on Si, where molecules in higher layers stand up on the surface. As the metallic character of a surface was suspected to be decisive as regards whether molecules lie flat or stand up in higher layers, LEEM and PEEM studies were performed to clarify this dependence. Control over the metallicity was gained by using monolayer thick Au films on Si(111) as a substrate for the pentacene growth. This has the advantage that the substrate can be prepared in a very controlled manner, inside the microscope, directly prior to the deposition of the pentacene. The formation of submonolayer thin Au films on Si(111) has already been studied extensively in the past [30–35]. During deposition at a substrate temperature of ≈700 °C the Si(111) (7×7) reconstruction is replaced by a Au-(5×2) phase [30]. At a Au coverage of 0.5 atomic layers (ML) [34], the entire surface is covered with this reconstruction. Further deposition leads to the observation of sharp Au-$(\sqrt{3} \times \sqrt{3})$ LEED spots in addition to the Au(5×2) LEED pattern. Coexistence of the two phases ends at a coverage of about 0.75 ML, when the entire surface is covered with Au-$(\sqrt{3} \times \sqrt{3})$. STM results suggest [34] that the Au-$(\sqrt{3} \times \sqrt{3})$ reconstruction contains a large number of domain walls which would be filled in with ongoing deposition. Deposition beyond 1 ML usually creates three-dimensional Au clusters on the surface [36]. Deposition of Au on Si(111) thus allows the controlled preparation of different surfaces, both a Au-(5×2) phase and a Au-$(\sqrt{3} \times \sqrt{3})$ phase.

Figure 8 shows the result of a room temperature pentacene deposition on the Au-(5×2) phase (a) and on the Au-$(\sqrt{3} \times \sqrt{3})$ (b) phase [37].

If pentacene is deposited on the Au-(5×2) reconstruction, fractal islands grow and the LEED pattern is similar to the

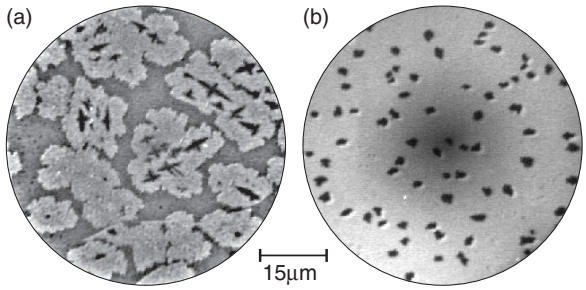

Figure 8. PEEM images of pentacene room temperature growth on Au/Si(111) substrates. (a) Growth on the Au(5 × 2) reconstruction; (b) growth on the Au($\sqrt{3} \times \sqrt{3}$) reconstruction. After [37].

growth of pentacene on Si. If, however, pentacene is grown on the Au-($\sqrt{3} \times \sqrt{3}$) reconstruction (that only contains 0.25 ML more Au than the Au-(5 × 2)), the result is completely different. In panel (b) of figure 8 only a few dark spots are visible on the surface, although many molecular layers of pentacene were deposited. The dark spots form at a very early stage during growth and their lateral dimension increases very slowly with ongoing deposition. *Ex situ* AFM measurements have shown that the dark spots represent whiskers that grow with a preferential direction perpendicular to the surface. These whiskers can easily reach lengths of several hundred nanometers. Figure 9(a) shows a close-up LEEM image of such whiskers. The larger whisker at the top of panel (a) exhibits the microdiffraction pattern in panel (b). The diffraction pattern of the whisker is obviously significantly different from the diffraction patterns of the thin film phase with molecules standing up in figure 5. The unit cell for the diffraction pattern of the whisker has been sketched in figure 9(b) and corresponds to lattice vectors of 15.7 and 6.5 Å, i.e., values that are close to the bulk *c* and *a* lattice constants of various bulk polymorphs [38–41]. Apparently, the molecules are in the case of pentacene on Au-($\sqrt{3} \times \sqrt{3}$) aligned parallel to the surface.

The large whisker at the top of figure 9(a) is connected to a smaller whisker at the bottom left of the same panel. The microdiffraction pattern of this whisker is shown in panel (c) of figure 9. A comparison of panels (b) and (c) reveals that the microdiffraction patterns of the large and small whisker are rotated with respect to each other by 120°, thus 'trying' to mimic the substrate threefold symmetry. Even if a large number of whiskers is analyzed, the pentacene crystal lattice will always align with the substrate.

It is puzzling that the small difference of 0.25 ML in coverage between the Au-(5 × 2) reconstruction and the Au-($\sqrt{3} \times \sqrt{3}$) reconstruction modifies the film's morphology so dramatically and induces a complete change of the adsorption geometry. Altmann *et al* [42] have analyzed the electronic structure of the Au-(5 × 2) and Au-($\sqrt{3} \times \sqrt{3}$) reconstructions in great detail and conclude that the higher coverage phase, Au-($\sqrt{3} \times \sqrt{3}$) is clearly metallic—in contrast to the lower coverage semimetallic Au-(5 × 2) phase. Apparently, it is the local density of states (LDOS) at the surface that is decisive as regards whether pentacene molecules on a surface lie down or stand up. This interpretation was supported [37] by the observation that pentacene molecules on a semimetallic Bi film also stand upright.

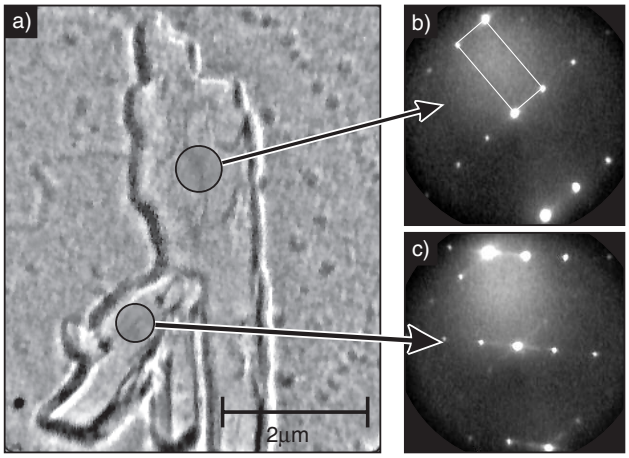

Figure 9. LEEM and LEED images of pentacene grown at room temperature on the Au($\sqrt{3} \times \sqrt{3}$)/Si(111) surface. (a) The bright-field LEEM image shows several pentacene whiskers; ((b), (c)) microdiffraction patterns show that each whisker is single crystalline and exhibits a LEED pattern that is different from the LEED pattern of the thin film phase. After [37].

3. Anthracene

Anthracene ($C_{14}H_{10}$) also belongs to the group of linear hydrocarbons and is composed of three aromatic rings. Anthracene has a singlet exciton in the blue part of the visible spectrum (E_{s1} = 3.1 eV [43]) and, accordingly, anthracene derivatives are used in blue organic light emitting diodes. Non-functionalized anthracene is much harder to handle experimentally than pentacene, as the vapor pressure of anthracene is so high that the samples need to be cooled in order to obtain film growth at all. Some of the PEEMs and LEEMs, however, have cooling options built into the microscope manipulator and provide for imaging of films at low temperatures during growth.

3.1. Growth on Si surfaces

Despite the fact that the bulk structure of anthracene (monoclinic) is different from the bulk structure of bulk pentacene (triclinic) [38, 39], the growth behavior is in general very similar. Anthracene, if deposited on Si(111) at a substrate temperature of $T \approx -40\,^{\circ}\mathrm{C}$, forms fractal islands with a size of tens of micrometers just like pentacene. Figure 10 shows the relative coverage of the first layer of anthracene as a function of the integral coverage [44], similar to figure 4 for pentacene. As in the case of pentacene, it takes some time after the beginning of the anthracene deposition for structural features to become visible in the PEEM images. During deposition, before islands are formed, the brightness of the PEEM image increases linearly, indicating that material is indeed deposited on the surface. After a total coverage of about 0.4 ML is deposited, dark fractal islands are formed. The percentage of the surface that is covered with these islands increases linearly

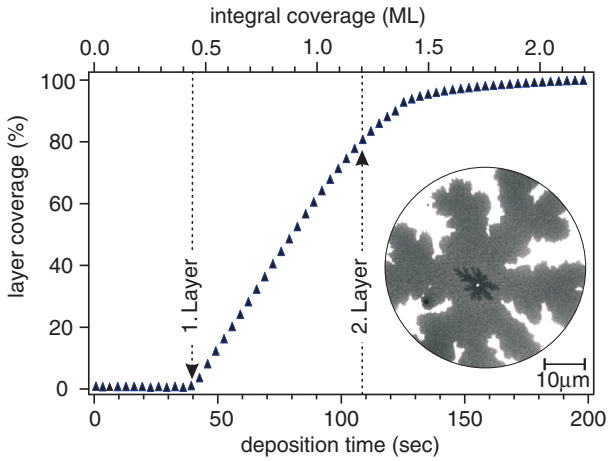

Figure 10. Relative coverage of anthracene in the first layers as a function of the deposition time. After the beginning of the deposition, more than 0.4 ML of anthracene are adsorbed on the surface before the first islands become visible. The inset is an over-exposure of the anthracene at a time after the deviation of the layer coverage from a straight line. After [44].

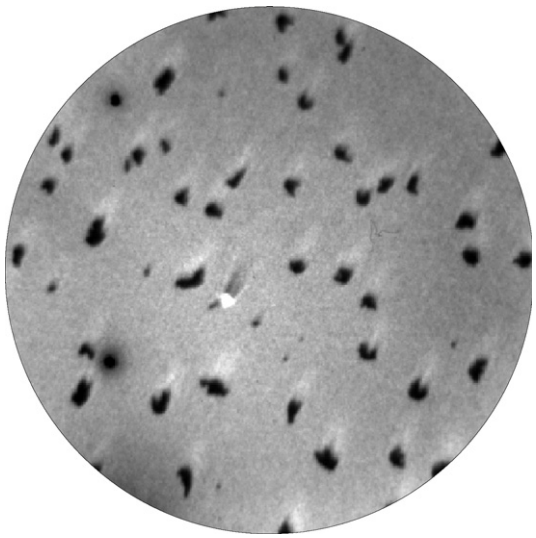

Figure 11. PEEM image of anthracene islands grown on Ag-($\sqrt{3} \times \sqrt{3}$)/Si(111). The field of view is 50 μm.

until an integral coverage of 1.2 ML is reached. Considering the bulk work function of anthracene of 5.65 eV [45], it is not surprising that anthracene islands appear black in PEEM under illumination with a Hg discharge lamp that only provides photons with an energy below 5 eV. This argument for the first layer implies, however, that higher layers will also most likely appear black, and that the first layer and the second layer cannot be distinguished in PEEM. The deviation from the linear behavior at an integral coverage of 1.2 ML in figure 10 is thus most likely due to the formation of a second layer. Over-exposure of the images in PEEM (see the inset in figure 10) renders the area between the islands white, the first layer gray, and the second layer black, and confirms this interpretation.

Using the same arguments as above for pentacene, it was concluded from the presence of a dead-time before nucleation of the first islands that in the case of anthracene a wetting layer of flat lying molecules is also formed, with molecules standing up in the first layer on top of this wetting layer. Although the growths of the two polyacenes, pentacene and anthracene, are very similar, the absolute value for the dead-time differs significantly. In the case of pentacene it was argued that a flat lying layer of molecules would cover the surface after a total coverage of 0.2 ML, as the molecule is approximately five times longer than it is wide, and the definition of the monolayer was given by the amount of molecules standing up that fit into one layer. Using the same argument for anthracene, one would come to the conclusion that the molecule is only three times longer than it is wide and one would expect a dead-time of 1/3 of a monolayer, not >40% of a monolayer. Apparently, as the argument underestimated the amount of anthracene in the flat layer, anthracene molecules seem to be packed more tightly in the first layer compared to the case for pentacene. It can only be speculated that the shorter molecule anthracene finds more binding sites on the surface and by using its rotational degree of freedom manages to deposit more atoms into the flat layer before the surface cannot accommodate further molecules and islands with molecules standing up are formed.

3.2. Metallic substrates

The similarities in the growth of anthracene and pentacene extend to the orientation of the molecules once deposited on metallic substrates. In this case, the Ag-($\sqrt{3} \times \sqrt{3}$) reconstruction has been used as a substrate [46], that can be prepared by deposition of Ag on Si(111) at substrate temperatures between 350 and 600 °C. The atomic configuration of this reconstruction with a honeycomb arrangement [47] is very similar to the Au-($\sqrt{3} \times \sqrt{3}$) reconstruction that is formed on the same Si surface. For pentacene, the electronic structure of the surface [48] has apparently sufficient metallic character to force pentacene molecules to lie down flat on the surface [49, 50]. The same holds for anthracene. Figure 11 shows a PEEM image of an anthracene deposit on the Ag-($\sqrt{3} \times \sqrt{3}$) surface at $T \approx -40$ °C. The resemblance of figure 11 to panel (b) of figure 8 is striking. Apparently, also anthracene molecules form whiskers on a metallic substrate.

4. Imaging of electronic states inside the molecules

Threshold photoemission PEEM provides images of the filled states of organic molecules, i.e., the HOMO and, if energetically possible, lower energy levels as well. For recombination-based devices like OLEDs, however, the electronic and optical transitions within the molecules are of interest. In particular, the HOMO–LUMO transition in OLEDs determines the wavelength, the intensity, and the polarization of the emitted light. To gain insight into the HOMO–LUMO transitions and to understand how the LUMO density of states is influenced by morphological features on the surface, it would be desirable to use PEEM to image the LUMO

level rather than the HOMO level. This endeavor can be achieved by exploiting nonlinear photoemission processes, i.e., by transferring electrons from the HOMO to the LUMO state via a first photon, and by subsequent photoemission from the now occupied LUMO state via a second photon. Since, in this case, two photons are required for each photoemitted electron, the photoemission yield Y in this two-photon photoemission (2PPE) process scales with the intensity I of the light [51] as $Y \propto I^2$. As a consequence, obtaining a sufficiently high photoelectron count rate demands a combination of intense light sources with PEEM. Only with the advent of femtosecond laser oscillators [52] did it become feasible to perform two-photon photoemission microscopy (2PPE-PEEM) [53, 54]. In most of today's 2PPE-PEEM experiments, mode-locked Ti:sapphire sources are used that can be purchased from various vendors. The mode-locked lasers typically provide <20 fs laser pulses with a pulse energy of a few nanojoules and a repetition rate of the pulses of 80 MHz.

Unfortunately, determined by the design of the femtosecond lasers, the range of possible wavelengths of the light pulses is limited to a spectral range around $\lambda = 800$ nm. Other wavelengths can be achieved by frequency doubling, or by amplification of the laser pulses in regenerative amplifiers and by using optical parametric amplifiers (OPAs). The latter is paid for with a much more complex optical setup and usually requires a reduction of the repetition rate to less than 100 kHz.

It must be emphasized here that many different processes can contribute to the 2PPE yield and that it depends on the specific system of interest which one of the possible processes provides the dominating contribution to the photoelectron yield. Metals, for example, have a continuum of states above the Fermi edge, and the behavior strongly differs from that of the molecular systems with discrete energy levels that are discussed here. Also, plasmon resonances [55], surface plasmon–polariton waves [56], and near-field effects [57, 58] can influence the photoemission yield.

To facilitate discussion of 2PPE-PEEM imaging of organic thin films, a compilation of regular PEEM and 2PPE-PEEM images of thin films of pentacene and anthracene is displayed in figure 12. The films, of which images are shown in figure 12, were again grown on Si substrates, i.e., the films consist of a flat lying and disordered wetting layers with molecules standing up on top of the flat layer that assemble into crystalline islands.

The two upper panels of figure 12 show regular PEEM images obtained under illumination with the Hg discharge lamp. As already discussed, for pentacene the (almost closed) first layer is brighter than the background, and the second layer appears darker than the first layer. In the case of anthracene the background is bright and the islands are dark, due to the significantly higher work function of anthracene compared to pentacene. The two panels (c) and (d) at the bottom of figure 12 each show the same area on the surface as is displayed in the panels above them, but the bottom panels were obtained under illumination with frequency doubled, $\lambda = 400$ nm laser pulses. It was verified for both pentacene and anthracene that photoemission in this case does indeed take place via a two-photon photoemission process. This was accomplished

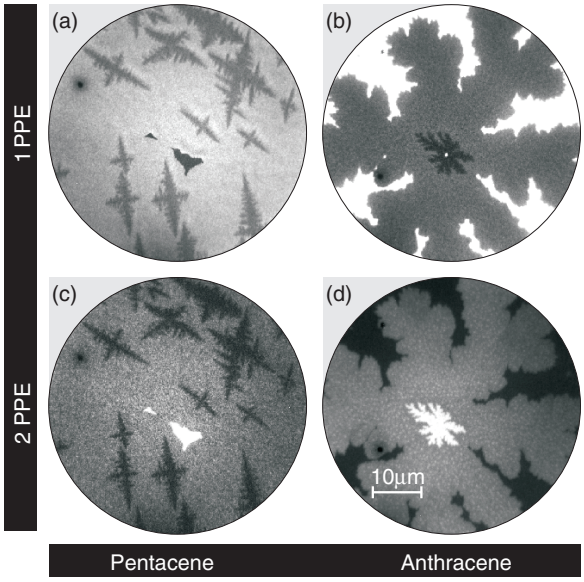

Figure 12. Comparison of regular (threshold) photoemission and two-photon photoemission for thin films of pentacene and anthracene grown on Si substrates. The panels at the bottom show the same area on the surface as the panels at the top. The field of view is 50 μm for all panels.

by recording a sequence of PEEM images at different laser intensities and by confirming the $Y \sim I^2$ yield dependence that is indicative of the 2PPE process. Furthermore, to ensure that photoemission proceeds via 2PPE for all areas on the surface, the exponent of the power law was determined for every pixel in a sequence of PEEM images and mapped out over the surface (power mapping [59]). A homogeneously gray power map without any structure and a value of the exponent of 2 for all pixels confirms that the photoemission process is homogeneous over the surface and not dependent on morphological features.

If one compares the panels at the top of figure 12 to the panels at the bottom, it is obvious that the contrast is different for regular PEEM and 2PPE-PEEM. Since the pairs of panels (a) and (c) and panels (b) and (d) originate from the same area on the surface, a direct comparison between the top panels (PEEM) and the bottom panels (2PPE-PEEM) can be drawn. It is interesting to note, however, that even qualitatively the change in contrast differs for pentacene and anthracene. In figure 12(c) the 2PPE-PEEM image of the pentacene film renders the wetting layer of flat lying molecules the brightest, while the higher layers become continuously darker. The 2PPE-PEEM signal of anthracene, displayed in panel (d) of figure 12, is simply inverted from the threshold photoemission case. Here the islands are brighter in 2PPE than in threshold photoemission (although it will be demonstrated below that the actual brightness of an anthracene island is a function of the polarization of the laser pulses).

The 2PPE-PEEM contrasts of anthracene and pentacene are caused by the differences in electronic structure of the molecules and can be understood if the HOMO–LUMO gaps of the molecules are considered. Figure 13 shows the dependence of the maximum of the optical adsorption of the

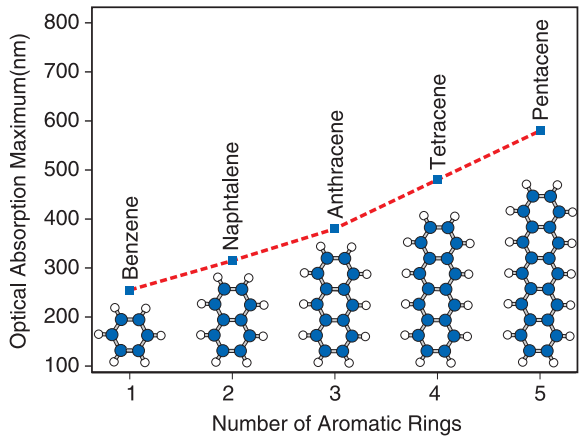

Figure 13. The maximum of the optical adsorption as a function of the chain length of the polyacenes for bulk crystals. Data after [60, 61].

linear conjugated molecules as a function of the number of aromatic rings of the molecules for bulk crystals [60, 61]. The maximum of the optical absorption systematically depends on the chain length. For short molecules the maximum of the optical absorption lies in the ultraviolet, and for longer molecules it shifts into the infrared. As the optical absorption is linked to the possible electronic excitations in the molecules, figure 13 can form the basis for a discussion of the 2PPE-PEEM contrast for pentacene and anthracene.

For pentacene bulk, the maximum of the optical absorption lies in the infrared, which corresponds to the HOMO–LUMO gap of the molecule. For the thin film phase, the HOMO–LUMO gap has an energy of ∼1.9 eV [62], slightly different from the bulk value. For the bulk as well as for thin films, however, the femtosecond laser pulses, with a wavelength of $\lambda_0 = 400$ nm and a spectral width of 15 nm, i.e., a photon energy in the range of 3.1 ± 0.05 eV, excite electrons from the HOMO level into higher unoccupied orbitals. The density of states in these higher orbitals is low [62] and as a result the 2PPE process is ineffective and the 2PPE yield is small.

For anthracene, on the other hand, the HOMO–LUMO gap is ≈4 eV in the bulk, significantly larger than the bandgap of pentacene; in fact, it is so large that the $\lambda_0 = 400$ nm laser pulses cannot cause a HOMO–LUMO transition in the bulk. Anthracene, however, has two exciton states at energies that are slightly lower than the HOMO–LUMO gap. As these excitons are relevant for anthracene-based OLEDs, they have been extensively investigated with optical methods. For bulk anthracene, the first singlet exciton S_1 is located at $E = 3.1$ eV [63]. The S_1 exciton, however, can only be excited by a laser pulse that has its electric field aligned with the *b*-axis of the anthracene unit cell [64]. Excitation with electric fields along the *a*- or *c*-axis would require light with an energy of $E = 3.3$ eV [65] or $E = 4.2$ eV (S_2 exciton) [64], respectively. Apparently, only the singlet exciton S_1 with an excitation energy of 3.1 eV is relevant for the 2PPE process as it perfectly matches the photon energy of the laser pulses. Once

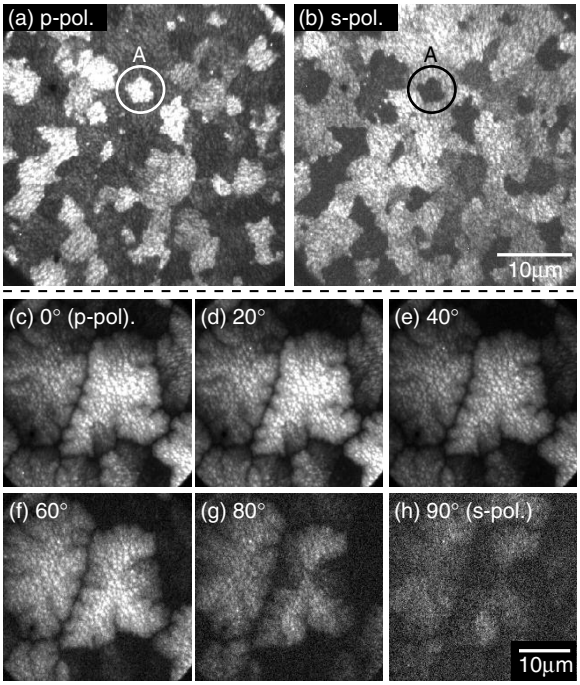

Figure 14. The brightness of anthracene islands in 2PPE-PEEM for different polarizations of the fs laser pulses. (a) Islands under p polarization, (b) islands under s polarization. The circle labeled 'A' marks the same island in both panels. ((c)–(h)) 2PPE yield of a larger anthracene island as a function of the polarization angle. The brightness of the panels has been adjusted to resemble similar grayscales. The contrast between the island and the background vanishes at s polarization.

the exciton has been excited, photoemission can take place during the absorption of the second photon in 2PPE-PEEM.

Since the S_1 exciton can only be excited with an electric field along the *b*-axis of the film, a strong dependence of the 2PPE signal on the polarization of the laser is expected. Whenever the electric field of the laser is aligned with the *b*-axis of the film, a high photoemission yield is expected, while in the case of an electric field perpendicular to the *b*-axis, a minimal photoemission yield is expected. Figure 14 illustrates the dependence of the 2PPE signal on the polarization of the laser pulses. The polarization of the laser pulses is adjusted by a $\lambda/2$ waveplate, and the pulses hit the sample in a grazing incidence geometry under an angle of 74° with respect to the surface normal. As a consequence, in p polarization the electrical field vector has a component within the surface plane and a component perpendicular to the surface plane as well [55]. For the excitation of the S_1 exciton, however, the out-of-plane component does not play a role since for a film of anthracene molecules standing up the *b*-axis of the unit cell lies within the surface plane. In the case of s polarization, the electric field vector lies completely in the surface plane, and the in-plane component of the s-polarized laser pulses is rotated by 90° compared to the case for p polarization.

Panel (a) of figure 14 shows a Si(111) surface with many anthracene islands, each about 5 μm large, under illumination with p-polarized laser pulses. Although the whole surface is covered with islands, each island exhibits a different

brightness. The circle labeled 'A' marks a bright island that is surrounded by dark islands. Panel (b) of figure 14 shows the same area on the surface as displayed in panel (a), but under illumination with s-polarized laser pulses, i.e., the in-plane component of the electric field is rotated by 90° compared to panel (a). The marker island 'A' appears dark now, and all other islands display a different brightness than they do in panel (a), as well. The smaller panels (c)–(h) at the bottom of figure 14 show the dependence of the 2PPE yield on the polarization in more detail for a single island. Under p polarization the island appears bright and gradually gets darker when the direction of the electric field is rotated. From a detailed analysis of the 2PPE yield of the islands as a function of the polarization angle, the orientation of the *b*-axis of the unit cells for each of the islands can be reliably determined. A statistical analysis of the 2PPE yield as a function of the polarization angle shows an arbitrary distribution of the azimuthal orientation of the islands. This observation is similar to the case for pentacene, where a random azimuthal distribution was concluded from LEED measurements. Furthermore, anthracene islands that form on top of an already present anthracene island show the same polarization dependence as the islands on which they were formed, clearly indicating an epitaxial relationship between higher anthracene layers and the underlying film.

5. Conclusions

PEEM and LEEM are excellently suited to studying the growth and properties of organic thin films. The fantastic capability for studying the growth of the films during deposition provides a promising perspective for understanding the growth dynamics of organic thin films in detail. LEED and microdiffraction allow determining the crystalline structure and orientation even for small islands, and PEEM provides the toolkit for investigating the local electronic structure of the films. Using pulsed lasers even extends the methodology to studying excited states inside the molecules, and measurements of excitation lifetimes and hot electron dynamics with spatial resolution in pump–probe experiments have been recently demonstrated for pentacene and anthracene as well.

The downside of this exciting method is, however, that not all organic molecules are suitable for LEEM and PEEM studies, and the two techniques, powerful as they may be, cannot provide all the answers. First of all, organic molecules that are suitable for LEEM and PEEM must be somewhat UHV compatible. This already excludes a wide range of materials. In some cases, it is possible to use lower deposition temperatures to force the molecules onto the surface, as in the anthracene case, but more frequently the lower temperatures will create an environment that is different from the environment in which the molecule will later be used. For instance, it is possible to image liquid crystal droplets in PEEM, but the shape of the droplets changes over time as the material desorbs and balls up due to its surface tension. Freezing of the droplets would force them onto the surface and stabilize then, but it will also trigger crystallization and change the material itself—thus making it questionable to what extent the findings are relevant for liquid crystal applications.

A second restriction for organic molecules in LEEM and PEEM is that the films must be somewhat conductive, as must be the substrates. Since a bias voltage of ∼20 kV must be applied to the sample surface, isolators are usually not suitable for observation in LEEM and PEEM and provoke HV arcing between the sample and the objective lens. The commonly used glass or mica substrates for organic films are thus not suited as substrates for LEEM and PEEM but can be replaced by thin SiO_2 layers that exhibit a sufficiently high leakage current.

The third restriction is of a somewhat more fundamental nature: the molecules have to form structures that are large enough to be resolved by the microscopes. For new commercial LEEM instruments, the state-of-the-art resolution lies around 4–5 nm and structures that are not significantly larger will be impossible to resolve with LEEM or PEEM. This implies that amorphous films will appear homogeneously gray in LEEM and PEEM, which makes the method rather unattractive for most polymer films. Other molecules form large enough islands for identifying the structures that they form laterally, but the thickness of the layers may be unknown—the growth might not even proceed in a layer by layer fashion. An example showing such a lack of vertical contrast in PEEM is provided by the dark pentacene whiskers on the Au $(\sqrt{3} \times \sqrt{3})$/Si(111) reconstruction in figure 8(b), in which the height of the layers cannot easily be determined in the PEEM, although *ex situ* AFM shows that the whiskers are at least 100 nm high. Anthracene growth on Si is another candidate for showing the lack of vertical information: here, first-layer islands appear black due to their high work function. Accordingly, the second layer can hardly be distinguished from the first layer. Similar observations were made with C_{60} on Bi [66] and C_{60} on Ag. In these cases, however, the nucleation process can still be analyzed, and if the molecules assemble into sufficiently large structures, the growth behavior of the first layer is also accessible.

Only in the cases where the electronic properties of the molecular layer are a function of the film's thickness and the molecules order into structures with a size sufficiently large for the microscopes can studies of the growth dynamics be carried out reliably for films that are several layers thick. Pentacene and PTCDA [67] have proven to be prime candidates for such studies. Anthracene on first glimpse is not, because the layers could not be distinguished in PEEM. However, by the choice of a different light source and by exploiting 2PPE processes, it was possible to distinguish the anthracene layers and to follow the growth in light of the S_1 exciton state. This last example illustrates that in PEEM the actual contrast that can be obtained depends on several factors, the choice of light source maybe not being the most obvious one, but being one of the most important ones. PEEMs and LEEMs that are installed at user facilities all over the world have a wide variety of wavelengths for spatially resolved core level and valence band spectroscopy available. For many molecules, the proper choice of wavelength for the illumination will result in contrast that is suitable for helping provide insight into the growth properties of organic molecules.

Acknowledgments

The author is grateful for the support from colleagues at IBM Research and the University of Duisburg-Essen who have, over the years, contributed to the results that form the basis of this article. Financial support is acknowledged from the Humboldt Foundation for a Feodor Lynen Fellowship and from the Deutsche Forschungsgemeinschaft within the Collaborative Research Center SFB 616: 'Energy Dissipation at Surfaces'.

References

[1] Tromp R, Mankos M, Reuter M, Ellis A and Copel M 1998 *Surf. Rev. Lett.* **5** 1189
[2] Schmidt T, Heun S, Slezak J, Diaz J, Prince K, Lilienkamp G and Bauer E 1998 *Surf. Rev. Lett.* **5** 1287
[3] Grzelakowski K and Bauer E 1996 *Rev. Sci. Instrum.* **67** 742
[4] Grzelakowski K 1999 *Rev. Sci. Instrum.* **70** 3346
[5] Bauer E 1994 *Surf. Sci.* **299/300** 102
[6] Bauer E 1994 *Rep. Prog. Phys.* **57** 895
[7] Tromp R M 2000 *IBM J. Res. Dev.* **44** 503
[8] Wichtendahl R *et al* 1998 *Surf. Rev. Lett.* **5** 1249
[9] Meyer zu Heringdorf F, Reuter M and Tromp R 2004 *Appl. Phys.* A **78** 787
[10] Meyer zu Heringdorf F-J, Reuter M and Tromp R 2001 *Nature* **412** 517
[11] Mattheus C, Dros A B, Baas J, Oostergetel G, Meetsma A, de Boer J and Palstra T 2003 *Synth. Met.* **138** 475
[12] Dimitrakopoulos C, Brown A and Pomp A 1996 *J. Appl. Phys.* **80** 1996
[13] Hughes G, Carty D and Cafolla A 2005 *Surf. Sci.* **582** 90
[14] Kasaya M, Tabata H and Kawai T 1998 *Surf. Sci.* **400** 367
[15] Kasaya M, Tabata H and Kawai T 1998 *Surf. Sci.* **406** 302
[16] Weidkamp K, Hacker C, Schwartz M, Cao C, Tromp R and Hamers R 2003 *J. Phys. Chem.* B **107** 11142
[17] Kury P, Roos K, Horn-von Hoegen M and Meyer zu Heringdorf F-J 2008 *New J. Phys.* **10** 23037
[18] Kury P, Roos K R, Thien D, Möllenbeck S, Wall D, Horn-von Hoegen M and Meyer zu Heringdorf F-J 2008 *Org. Electron.* at press doi:10.1016/j.orgel.2008.02.006
[19] Ruiz R, Mayer A, Malliaras G, Nickel B, Scoles G, Kazimirov A, Kim H, Headrick R and Islam Z 2004 *Appl. Phys. Lett.* **85** 4926
[20] Sadowski J, Sazaki G, Nishikata S, Al-Mahboob A, Fujikawa Y, Tromp R and Sakurai T 2007 *Phys. Rev. Lett.* **98** 046104
[21] Venables J, Spiller G D T and Hanbücken M 1984 *Rep. Prog. Phys.* **47** 399
[22] Ruiz R, Nickel B, Koch N, Feldman L, Haglund R J, Kahn A, Family F and Scoles G 2003 *Phys. Rev. Lett.* **91** 136102
[23] Wu R, Toccoli Y, Koch N, Iacob E, Pallaoro A, Rudolf P and Ianotta S 2007 *Phys. Rev. Lett.* **98** 076601
[24] Pratontep S, Brinkmann M, Nüesch F and Zuppiroli L 2004 *Phys. Rev.* B **69** 165201
[25] Pratontep S, Nüesch F, Zuppiroli L and Brinkmann M 2005 *Phys. Rev.* B **72** 085211
[26] Witten T and Sander L 1981 *Phys. Rev. Lett.* **47** 1400
[27] Schroeder P G, France C B, Park J B and Parkinson B A 2002 *J. Appl. Phys.* **91** 3010
[28] Söhnchen S, Lukas S and Witte G 2004 *J. Chem. Phys.* **121** 525
[29] Wang Y L, Ji W, Shi D X, Du S X, Seidel C, Ma Y G, Gao H-J, Chi L F and Fuchs H 2004 *Phys. Rev.* B **69** 075408
[30] Lipson H and Singer K 1974 *J. Phys. C: Solid State Phys.* **7** 12
[31] Chester M and Gustafsson T 1990 *Phys. Rev.* B **42** 9233
[32] Tanishiro Y and Takayanagi K 1989 *Ultramicroscopy* **31** 20
[33] Shibata M, Sumita I and Nakajima M 1998 *Phys. Rev.* B **57** 2310
[34] Nagao T, Hasegawa S, Tsuchie K, Ino S, Voges C, Klos G, Pfnür H and Henzler M 1998 *Phys. Rev.* B **57** 10100
[35] Seifert C, Hild R, von Hoegen M H, Zhachuk R and Olshanetsky B 2001 *Surf. Sci.* **488** 233
[36] Horn-von Hoegen M, Meyer zu Heringdorf F-J, Kähler D, Schmidt T and Bauer E 1998 *Thin Solid Films* **336** 16
[37] Thayer G, Sadowski J, Meyer zu Heringdorf F-J, Sakurai T and Tromp R 2005 *Phys. Rev. Lett.* **95** 256106
[38] Campbell R, Robertson J and Trotter J 1961 *Acta Crystallogr.* **14** 705
[39] Campbell R, Robertson J and Trotter J 1962 *Acta Crystallogr.* **15** 289
[40] Holmes D, Kumaraswamy S, Matzger A and Vollhardt K 1999 *Chem. Eur. J.* **5** 3399
[41] Mattheus C, Dros A, Baas J, Meetsma A, de Boer J and Palstra T 2001 *Acta Crystallogr.* C **57** 939
[42] Altmann K N, Crain J N, Kirakosian A, Lin J-L, Petrovykh D Y, Himpsel F and Losio R 2001 *Phys. Rev.* B **64** 035406
[43] Meyer Y, Astier R and Leclercq J 1972 *J. Chem. Phys.* **56** 801
[44] Buckanie N and Meyer zu Heringdorf F-J 2007 *Surf. Sci.* **601** 1701
[45] Lyons L and Morris G 1960 *J. Chem. Soc.* 5192–9
[46] Spiegel K 1967 *Surf. Sci.* **7** 125
[47] Ding Y, Chan C and Ho K 1991 *Phys. Rev. Lett.* **67** 1454
[48] Johansson L, Landemark E, Karlsson C and Uhrberg R 1989 *Phys. Rev. Lett.* **63** 2092
[49] Guaino P, Cafolla A, Carty D, Sheerin G and Hughes G 2003 *Surf. Sci.* **540** 107
[50] Guaino P, Cafolla A, McDonald O, Carty D, Sheerin G and Hughes G 2003 *J. Phys.: Condens. Matter* **15** 2693
[51] Aeschlimann M, Schmuttenmaer C A, Elsayed-Ali H, Miller R, Cao J, Gao Y and Mantell D 1995 *J. Chem. Phys.* **102** 8606
[52] Spence D, Kean P and Sibbett W 1991 *Opt. Lett.* **16** 42
[53] Schmidt I, Bauer M, Wiemann C, Porath R, Scharte M, Andreyev O, Schönhense G and Aeschlimann M 2002 *Appl. Phys.* B **74** 223
[54] Meyer zu Heringdorf F-J, Chelaru L, Möllenbeck S, Thien D and Horn-von Hoegen M 2007 *Surf. Sci.* **601** 4700–5
[55] Chelaru L, Horn-von Hoegen M, Thien D and Meyer zu Heringdorf F-J 2006 *Phys. Rev.* B **73** 115416
[56] Chelaru L and Meyer zu Heringdorf F-J 2007 *Surf. Sci.* **601** 4541
[57] Cinchetti M, Gloskovski A, Nepijko S, Schönhense G, Rochholz H and Kreiter M 2005 *Phys. Rev. Lett.* **95** 047601
[58] Aeschlimann M, Bauer M, Bayer D, Brixner T, Garcia de Abajo F, Pfeiffer W, Rohmer M, Spindler C and Steeb F 2007 *Nature* **446** 301
[59] Schmidt O, Fecher G, Hwu Y and Schönhense G 2001 *Surf. Sci.* **482–485** 678
[60] Tavan P and Schulten K 1979 *J. Chem. Phys.* **70** 5414
[61] Pope M and Swenberg C 1999 *Electronic Processes in Organic Crystals and Polymers* (New York: Oxford Scientific Publications)
[62] Tiago M, Northrup J and Louie S 2003 *Phys. Rev.* B **67** 115212
[63] Braun C L 1968 *Phys. Rev. Lett.* **21** 215
[64] Kobayashi M, Mizuno K and Matsui A 1989 *J. Phys. Soc. Japan* **58** 809
[65] Schwoerer M and Wolf H C 2005 *Organische Molekulare Festkoerper* (Berlin: Wiley–VCH)
[66] Sadowski J, Bakhtizin R, Oreshkin A, Nishihara T, Al-Mahboob A, Fujikawa Y, Nakajima K and Sakurai T 2007 *Surf. Sci. Lett.* **601** L136
[67] Marchetto H, Groh U, Schmidt T, Fink R, Freund H-J and Umbach E 2006 *Chem. Phys.* **325** 178